CHAPTER VI

THE EFFECTS OF FIRING TEMPERATURES ON PHASE FORMATION, MICROSTRUCTURE AND DIELECTRIC PROPERTIES OF $Bi_{0.5}(Na_{0.74}K_{0.16}Li_{0.10})_{0.5}TiO_3$ CERAMICS SYNTHESIZED VIA THE COMBUSTION ROUTE

Introduction

Lead-free piezoelectric ceramics have attracted increasing attention because the PbO in lead piezoelectric ceramics is volatile and detrimental to human health and the environment. Bismuth sodium titanate ($(Bi_{0.5}Na_{0.5})TiO_3$, BNT), discovered by Smolensky, et al. in 1960 [36], is one of the most important lead-free piezoelectric materials. This ceramic shows strong ferroelectricity of P_r = 38 μC/cm^2 and high Curie point of T_c= 540 °C [12]. However, because of its high coercive field (E_c = 73 kV/mm) and relatively large conductivity, pure BNT is difficult to be poled and is limited in its typical applications [68]. This is because both Bi and Na at the A-site of ABO_3 perovskite tend to evaporate during sintering at high temperature. Therefore, A-site vacancies should be easily formed in BNT ceramics and effect the conductivity of the materials [69].

Many researchers have attempted to improve BNT-properties by selecting some cation substituted on the A- site of a BNT system [70, 71, 72, 73, 74, 75]. Yang, et al. [70] studied the effects of K substituted to Na at the A-site of BNT perovskite in a range of 10-20 mol% on crystal structure, microstructure and electrical properties. The results indicated 18 mol% of K substitution induced an occurrence in the MPB region between the rhombohedral-tetragonal phases, which enhanced the dielectric properties of the ceramics. Lin, et al. [75] demonstrated that a small amount of Li could decrease sintering temperature and improve the densification of BNT-BT ceramics. The study on Li and K substituted BNT was extensively investigated by Lu, et al. [12]. The XRD results indicated that the $Bi_{0.5}(Na_{0.74}K_{0.16}Li_{0.10})_{0.5}TiO_3$ or BNKL1610 composition showed the coexistence of a rhombohedral and tetragonal structure which suggests this composition is located near the MPB region. Moreover,

the substitution of Li and K for BNKL1610 greatly improved the electrical properties of BNT such as increasing d_{33} from 78 to 160 pC/N, increasing k_p from 0.16 to 0.35 and increasing ε_r from 420 to 1080.

In terms of the preparation process, BNT-based ceramics were fabricated via the solid-state reaction method [14, 76]. The raw materials were heat treated at 800-900 °C for 2-5 h in a calcination process and at 1,050-1,200 °C for 2-5 h in sintering process [14, 76]. The secondary phases were formed due to the vaporization of raw materials at high temperature in the preparation processes [14]. To avoid this problem, BNT and BNT-based ceramics have been prepared by several wet chemical methods such as the sol-gel route [77], the hydrothermal method [78] and the molten salt synthesis [79]. However, it is well known that these chemical methods require a long processing time, special equipment and have a complex procedure [21].

Recently, the combustion technique has become an attractive technique to prepare ferroelectric materials because it's uncomplicated [20, 21, 52, 53]. Moreover, the released energy from fuel decomposition helps to reduce the firing temperatures in the preparation process. Therefore, the purpose of this study was to synthesize BNKLT1610 ceramics via the combustion route. The effects of firing temperatures on phase formation, microstructure and dielectric properties of BNKLT1610 ceramics were also investigated.

Experimental procedure

The starting chemicals for producing $Bi_{0.5}(Na_{0.74}K_{0.16}Li_{0.10})_{0.5}TiO_3$ or (BNKLT1610) ceramics were reagent grade bismuth oxide (Bi_2O_3), sodium carbonate (Na_2CO_3), potassium carbonate (K_2CO_3) , lithium carbonate (Li_2CO_3) and titanium oxide (TiO_2). The raw materials were weighed and mixed by ball milling in ethanol for 24 h. After the raw materials were dried and ground into fine powders, they were mixed with urea (CH_4N_2O) in a ratio of 1:2 in an agate mortar. The starting materials were calcined at various calcination temperatures ranging from 600 to 900 °C for 2 h. The X-ray diffraction (XRD) was employed to identify the phase formation and the optimum firing temperature for the prepared powders. Calcined powders obtained from appropriate condition were selected to press into pellets of 15 mm in diameter using uniaxial pressing in a stainless steel mold. The pellets were subsequently

sintered between 950 and 1,150 °C with a dwell time of 2 h. The phase formation behavior of the sintered ceramics was characterized by the X-ray diffraction pattern. The microstructure of the calcined powders was studied using transmission electron microscopy (TEM). SEM photographs were used to observe morphology and measure average particle size and grain size of the calcine powders and sintered ceramics. The bulk densities of the sintered samples were measured by the Archimedes method using distilled water as medium. Silver electrodes were applied on the opposite disk faces and were heated at 500 °C for 5 min. Dielectric measurement was carried out using a LCR meter connected to a PC.

Chemical compositions reaction

$$0.25Bi_2O_3 + 0.1875Na_2CO_3 + 0.04K_2CO_3 + 0.025Li_2CO_3 + TiO_2 \rightarrow Bi_{0.5}(Na_{0.74}K_{0.16}Li_{0.10})_{0.5}TiO_3 + 0.25CO_2 \quad \text{[Eq. 26]}$$

Results and discussion

Figure 59 shows the XRD patterns of the BNKLT1610 powders calcined at different temperatures from 600 to 900 °C. At a low calcination temperature (600 °C), the diffraction peaks can be indexed as the rhombohedral perovskite phase for BNKLT1610. This corresponded to the thermal analyzed by literature [14], which indicated that the BNT perovskite crystal can be formed above 500 °C. However, a small amount of the secondary phase of $M_2Ti_6O_{13}$ as described by Naderer, et al. [14] was detected. The formation of the secondary phase was caused by the volatilization of K_2O with high lead vacancies concentration as shown in Eq.27.

$$0.25Bi_2O_3 + 0.1875Na_2CO_3 + 0.04K_2CO_3 + 0.025Li_2CO_3 + TiO_2 \rightarrow Bi_{0.5}Na_{0.375}K_{0.08-x}Li_{0.05}V'_{(K)x}TiO_{3-(x/2)}V_{O(x/2)}\bullet\bullet + \frac{x}{2}K_2O + 0.25CO_2 \quad \text{[Eq.27]}$$

The evaporation of K_2O caused a shift in the A/B ratio of cation in composition. To reduces the number of vacancies and reduces the deviation of the A/B ratio, the secondary phase of $M_2Ti_6O_{13}$ was formed from starting materials as shown in Eq.28 where M refers to Na and/or Li and/or K [14].

$$M_2CO_3 + 6TiO_2 \rightarrow M_2Ti_6O_{13} + CO_2 \quad \text{[Eq.28]}$$

By increasing the calcination temperature, the secondary phase was decreased and completely eliminated when the calcination temperature reached 750 °C. The

calcining condition of 750 °C for 2 h, which produced pure the BNKLT1610 perovskite phase in this work was lower than that of the solid state reaction technique by 100 °C for 1 h [12]. This can be attributed to the energy released from the decomposition reaction of fuel which accelerated the chemical reaction of the raw materials [23, 24].The percentage of the perovskite phase was determined by measuring the major XRD peak intensities which were calculated and are listed in Table 15.

To determine the lattice parameter *a* of the rhombohedral structure (Table 15), the BNT crystal structure was assumed as a hexagonal structure and the lattice parameters *a* and *c* were calculated. Then, the *a* and *c* lattice parameters were transformed to a lattice parameter *a* of rhombohedral structure using the following equation [80];

$$a_R = \frac{1}{3}\sqrt{3(a_H)^2 + c_H^2} \qquad \text{[Eq.29]}$$

Where a_R is the lattice parameter of rhombohedral structure, a_H and c_H are the lattice parameters *a* and *c* of a hexagonal structure, respectively. The variation of lattice parameter *a* evinced the differences diffusion of cations into sub-lattices.

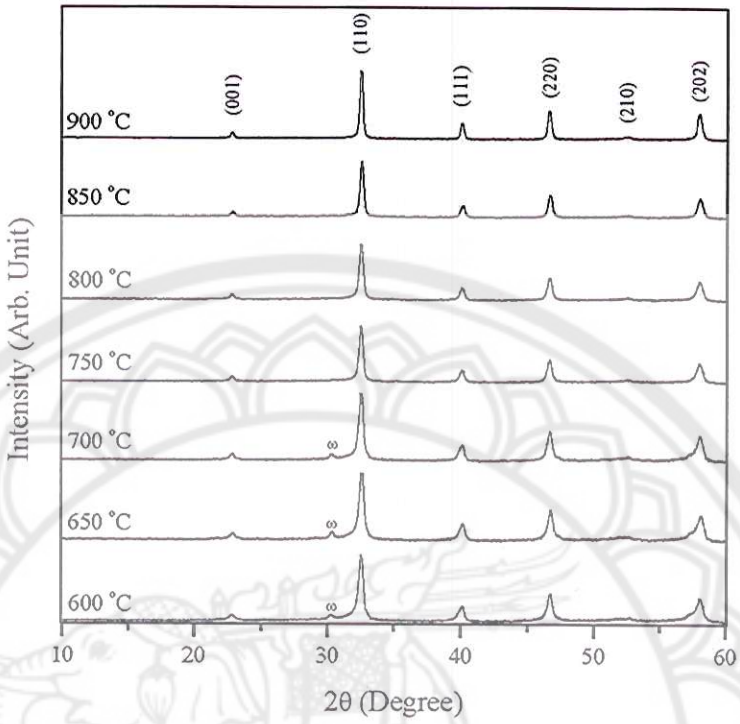

Figure 59 XRD patterns of BNKLT1610 powders calcined at different temperatures: (ω) $(K,Na,Li)_2Ti_6O_{13}$

The SEM photographs of BNKLT1610 powders calcined from 600 to 900 °C for 2 h are shown in Figure 60. The calcined powders consisted of fine particles, spherical shape and with an agglomerated form. Increasing the calcination temperature brought about a slight variation of particle size in the range of 110-360 nm as listed in Table 15. To obtain more particular characterizations, the TEM observation was investigated (Figure 61). When powders were calcined at a low temperature (Figure 61(a)), a dark zone appeared which indicated that electrons could not transmit through the multilayer of the sample. This demonstrated that a high agglomeration effect was induced. Increasing the calcination temperature up to 750 °C caused the agglomerated particles to be broken into fine individual particles (Figure 61(b)). The individual particles exhibited their particle size in the range of 100-200 nm, which is consistent with the SEM result. The individual particle shape was changed from a spherical to a cube shape when the calcination temperature was increased to 850 °C (Figure 61(c)). Moreover, many fine particles with a particle size lower than 100 nm were exhibited.

This indicated that the combustion technique is an effective route to produce BNKLT1610 nanopowders.

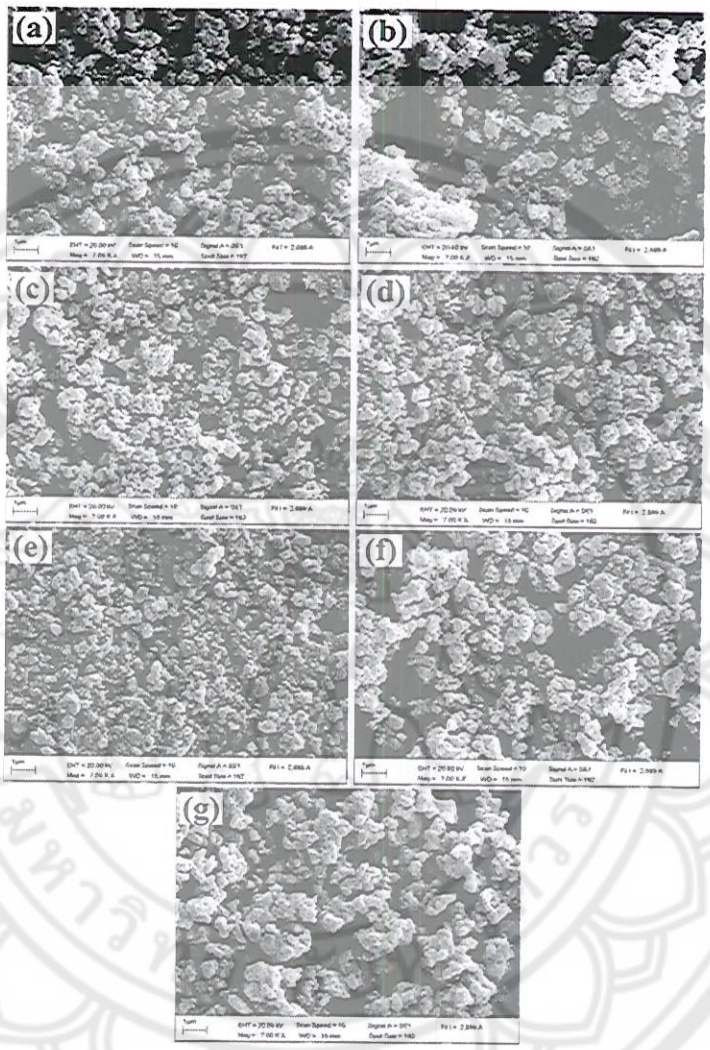

Figure 60 SEM photographs of BNKLT1610 powders calcined at; (a) 600 °C, (b) 650 °C, (c) 700 °C, (d) 750 °C, (e) 800 °C, (f) 850 °C and (g) 900 °C

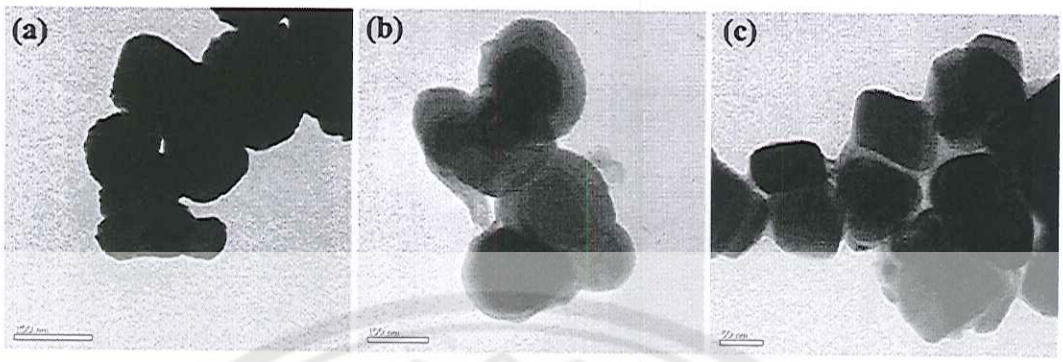

Figure 61 TEM micrographs of BNKLT1610 powders; (a) calcined at 650 °C, (b) calcined at 750 °C and (c) calcined at 850 °C

Table 15 Percent perovskite phase, lattice parameter *a* and average particle size of BNKLT1610 powders

Calcination temperature (°C)	% perovskite	Lattice parameter *a* (Å)	Average particle size (nm)
600	92.3	3.433	110
650	92.1	3.430	130
700	92.2	3.429	170
750	100	3.435	210
800	100	3.432	230
850	100	3.433	300
900	100	3.444	360

The powders calcined at 750 °C for 2 h were selected to fabricate the pellets and were sintered between 950 to 1,150 °C for 2 h. Figure 62(a) shows the XRD patterns of BNKLT1610 ceramics at various sintering temperatures. The pure perovskite phase was exhibited in ceramics sintered at 950 °C. By increasing sintering temperature up to 1,000 °C, the secondary phase of $M_2Ti_6O_{13}$ was repeatedly exhibited. The percentage of the perovskite phase was calculated and is listed in Table 16. Naderer, et al. [14] studied the secondary phase formation of $Bi_{0.5}Na_{0.375}K_{0.125}TiO_3$

ceramics. The results indicated that the ceramics initially decomposed at 990 °C and the secondary phase was formed at a temperature higher than 1,050 °C due to Bi_2O_3 and/or M_2O evaporating from the system. The formation of $M_2Ti_6O_{13}$ secondary phase at a high sintering temperature is described in Eq. 30.

$$16Bi_{0.5}M_{0.5}TiO_3 \rightarrow M_2Ti_6O_{13} + 10Bi_{0.5}M_{0.5}TiO_3 + \frac{3}{2}Bi_2O_3 + \frac{1}{2}M_2O \quad \text{[Eq. 30]}$$

The M-type could not be identified in this study. It is possible that M could be K and/or Li and/or Na. However, the secondary phase disappeared in the sample sintered at 1,150 °C. It is possible that it was volatized due to high firing temperature. This result is consistent with the literature which reports that the secondary phase in BKT decomposed at 1,120 °C [81].

The crystal structure of BNKLT1610 was investigated through XRD patterns which measured from 38 to 50° at a very low scanning rate (step size 0.00116°, time/θ 7.42 s, scan speed 0.05152 °/s) as is shown in Figure 62(b). Normally, BNT exhibits a rhombohedral structure (this is characterized by (003)/(021) peaks splitting at 2θ of 40° and a single peak of (202) at 2θ of 46.5°) whereas BKT exhibits tetragonal structure (which is a single peak of (111) at 2θ of 40° and splitting of (002)/(200) peaks at 2θ of 46.5°). Lu *et al.* [12] demonstrated that BNKLT1610 shows the coexistence of rhombohedral and tetragonal phases because its diffraction patterns showed splitting of (003)/(021) peaks at 2θ of 40° and splitting of (002)/(200) peaks at 2θ of 46.5° [12]. In this study, the BNKLT1610 ceramics sintered at 950 °C showed a slight splitting of (003)/(021) peaks at 2θ of 40° and an asymmetry peak of (200) at 2θ of 46.5°. So, this sample exhibited the mixed phases of rhombohedral-teragonal with the rhombohedral higher influenced on the crystal structure than the tetragonal phase. An increase of sintering temperature influenced the splitting of (003)/(021) peaks which decreased at 2θ of 40° while increasing the splitting of (200)/(002) peaks at 2θ of 46.5°. This indicated that the relative amounts of the tetragonal phases were increased. The splitting of diffraction peaks two positions 2θ of 40° and 46.5° was clearly observed in the sample sintered at 1,050 and 1,100 °C. This result indicated that the samples show the coexistence of rhombohedral and tetragonal phases. Moreover, increasing the sintering temperature to 1,150 °C caused the splitting of diffraction peaks at 2θ of 40° to decrease. This can be infers that the crystal structure

was slightly transformed to a tetragonal phase. The lattice parameter *a* of the sintered ceramics were calculated and are listed in Table 16.

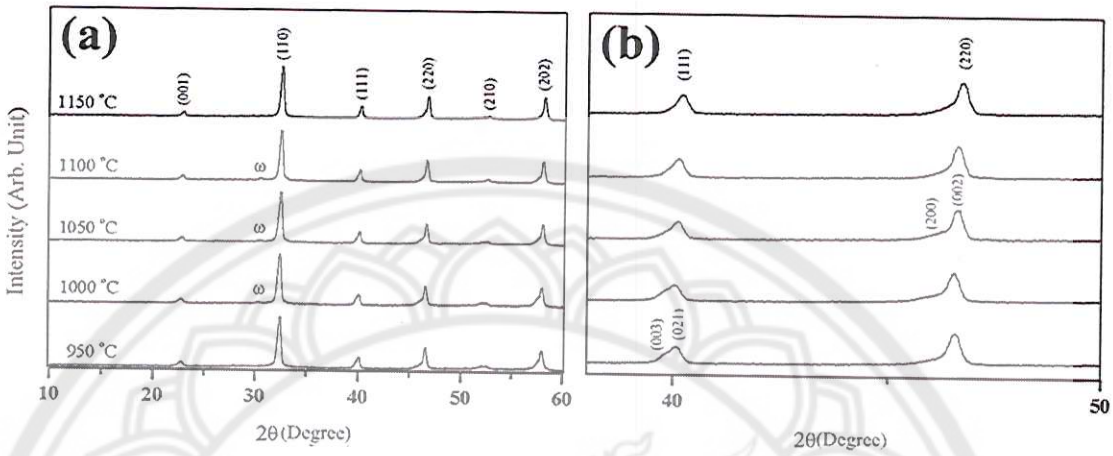

Figure 62 XRD patterns of BNKLT1610 ceramics sintered at various temperatures: (ω) $(K,Na,Li)_2Ti_6O_{13}$

Strong differences in the microstructure of the BNKLT1610 ceramics prepared at different sintering temperatures are seen in the SEM photographs in Figure 63. In the case of a low sintering temperature, the ceramics exhibited small grains with an irregular shape which represents the initial state of sintering (Figure 63(a)-(b)). Some of the melted plate was spread on the surface of the sample due to the evaporation of materials in the sintering process. By increasing the sintering temperature up to 1,050 °C (Figure 63(c)), the grain growth became increasingly active and the grain exhibited a quasi-cubic shape. However, the microstructure of the sintered ceramics showed a broad grain size distribution and many small grains exhibited initial grain growth characteristics. A narrow grain size distribution with clear grain boundaries, which is a feature of the grain growth process being nearly completed, is exhibited in the sample sintered at 1,100 °C for 2 h (Figure 63(d)). In addition, it should be noted that the surface micrograph of ceramics sintered at 1,150 °C shows evidence of melting grain, as can be seen in Figure 63(d). The variation of average grain size with increasing sintering temperatures was calculated and is listed in Table 16.

Figure 64 shows the SEM microstructures of the fracture surfaces of samples sintered with differences temperatures. Low sintering temperature brought about an

inadequate energy supply to the sample. Thus, the grains were weakened and transgranular fractures were exhibited (Figure 64(a) and (b)). By increasing the sintering temperature up to 1,050 °C, many intergranular fractures were observed as is shown in Figure 64(c). This indicates that the grains are sturdier than the grain boundaries. The intergranular fractures were distinctly observed when the sintering temperature was increased to 1,100 °C (Figure 64(d)). However, increase of sintered temperature to 1,150 °C caused the grain boundaries to be destroyed due to excessive heat (Figure 64(e)).

The measured density with a variation in sintering temperatures is listed in Table 16. The density of the ceramics was increased when sintering temperatures increased and reached its highest density at 1,100 °C with the value of 5.73 g/cm^3. Thereafter, the density decreased when the sintering temperature was increased to 1,150 °C. The reduction of density at high sintering temperature was caused by vitalization of the materials which induced high porosity in the sample. The density results corresponded with microstructure investigation. The highest density value of 5.73 g/cm^3 is higher than the density of 18 mol% K doped BNT ceramics (5.66 g/cm^3) [70] and slightly lower than the maximum density of K and Li doped BNT (5.76 g/cm^3) [82].

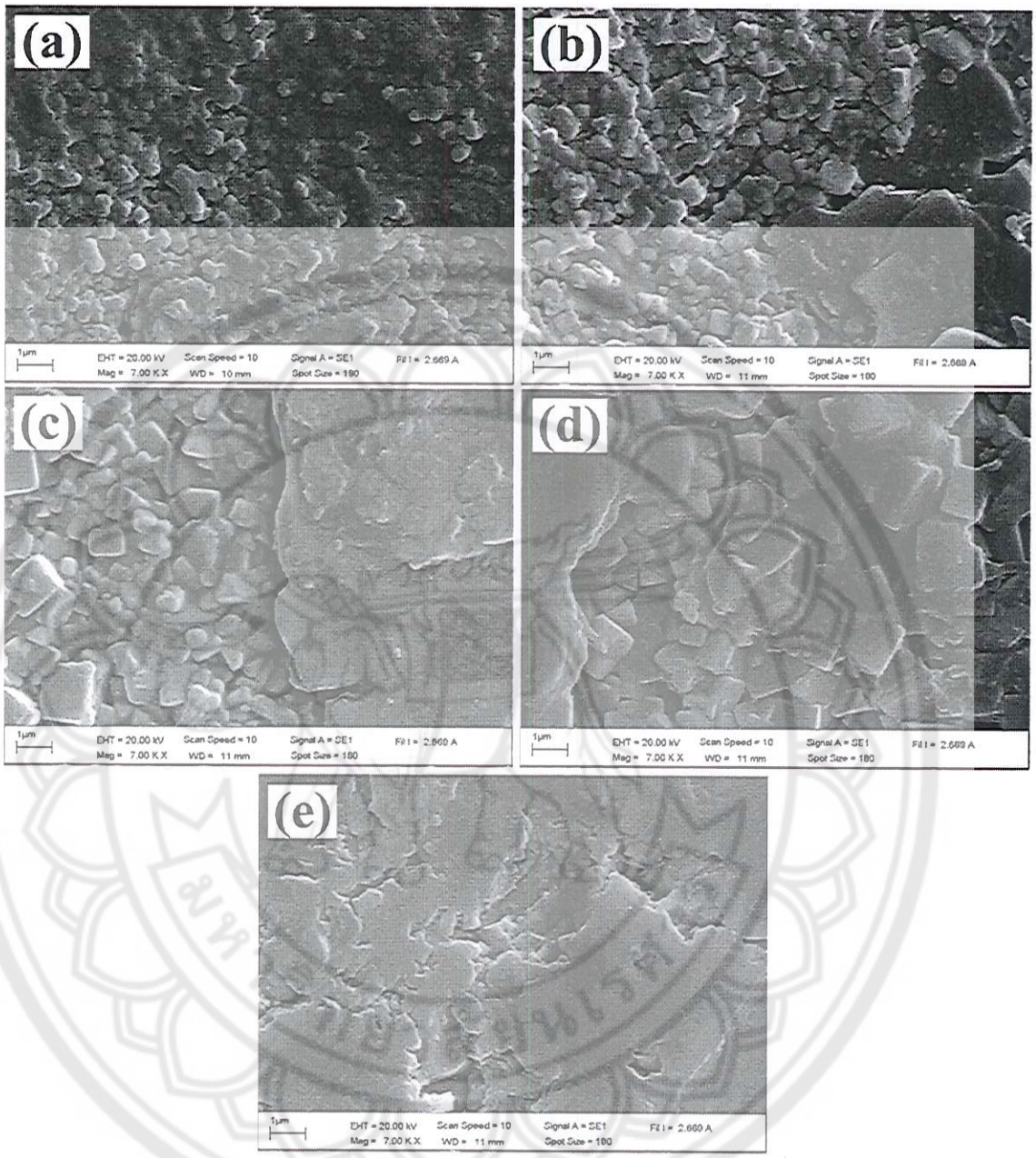

Figure 63 SEM photographs of surface BNKLT1610 ceramics sintered at; (a) 950 °C, (b) 1,000 °C, (c) 1,050 °C, (d) 1,100 °C and (e) 1,150 °C

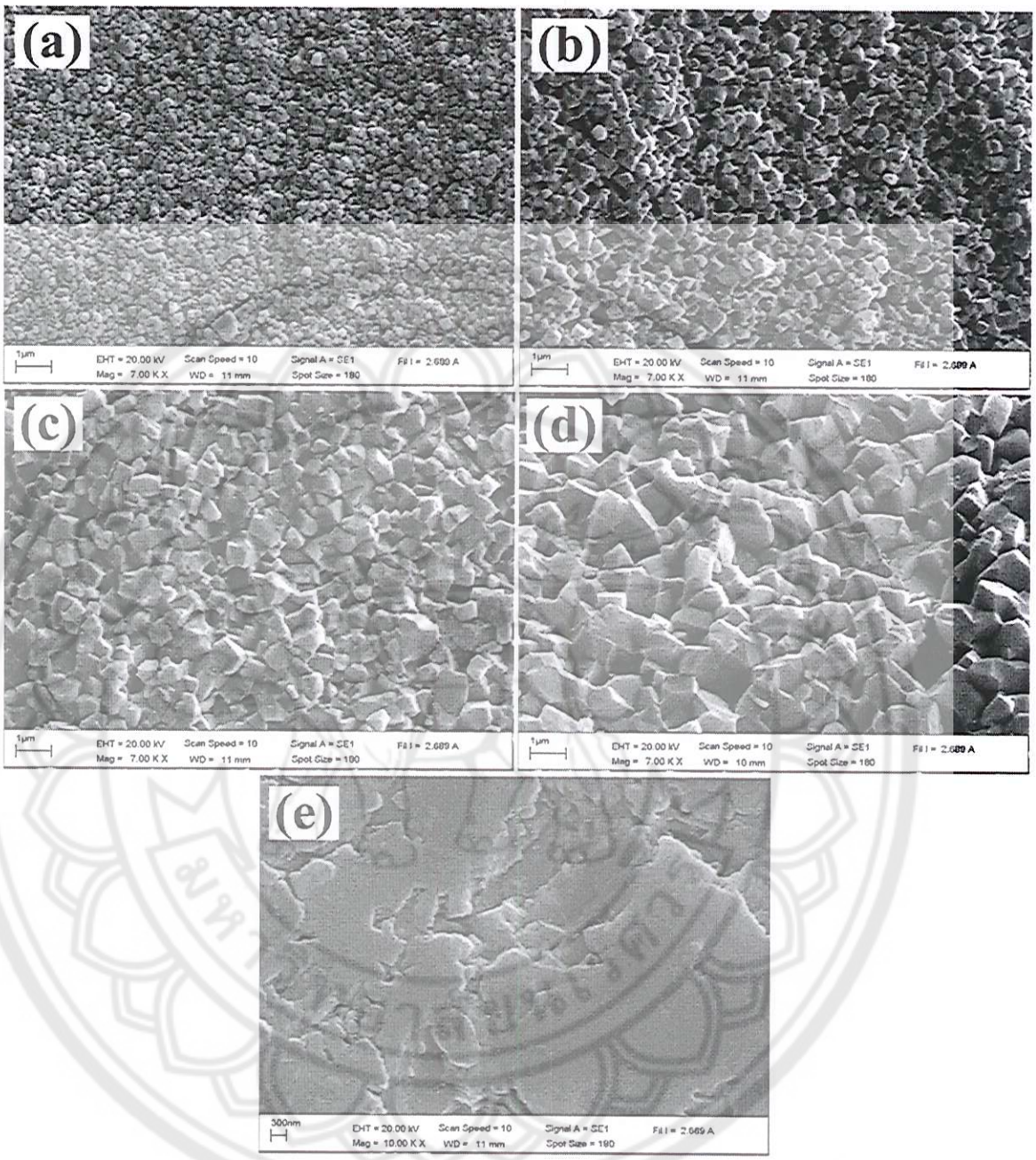

Figure 64 SEM photographs of fracture BNKLT1610 ceramics sintered at; (a) 950 °C, (b) 1,000 °C, (c) 1,050 °C, (d) 1,100 °C and (e) 1,150 °C

Table 16 Percent perovskite phase, lattice parameter *a*, average grain size and density of BNKLT1610 ceramics

Sintering temperature (°C)	Percent perovskite (%)	Lattice parameter *a* (Å)	Average grain size (nm)	Density (g/cm^3)
950	100	3.438	290	5.19
1,000	99.5	3.438	430	5.46
1,050	98.8	3.435	870	5.61
1,100	97.4	3.432	1,710	5.73
1,150	100	3.426	-	4.97

Figure 65 shows the temperature dependence of the dielectric constant and the tanδ of the BNKLT1610 ceramics sintered at various temperatures and measured at 1 kHz. Normally, the dielectric curve of BNT shows two distinct dielectric constant peaks at 125 and 320 °C. The first peak infers the phase transition from rhombohedral ferroelectric to a tetragonal anti-ferroelctric phase. The temperature at this phase transition point is called depolarization temperature (T_d). The next dielectric peak, which the dielectric constant shows its highest value, was observed at ~320 °C. This dielectric peak may be caused by the anti-ferroelctric phase transforming to the paraelctric phase and the temperature at this point is abbreviate as the maximum dielectric temperature (T_m). For this study, the BNKLT1610 ceramics sintered at 950 °C showed only one dielectric peak at temperature ~200 °C (T_d). The dielectric peak at T_m could not be observed. By increasing the sintering temperature to 1,000 °C, the dielectric peak at T_d distinctly appears. Moreover, a faint dielectric peak at a higher temperature (~320 °C) was observed. This is possibly the dielectric peak at T_m. The altitude of the dielectric peak at T_m is lower than the T_d altitude. The dielectric peak at T_m was more clearly observed when the sintering temperature increase to 1,050 °C. Increasing sintering temperature to 1,100 °C caused the dielectric peak at T_m to be distinctly exhibited and the maximum dielectric constant is observed at this point. For the sample sintered at 1,150 °C, the two dielectric peaks were clearly separated. The characteristics and position of the two dielectric peaks corresponded with the dielectric

curve of BNT ceramics reported by the literatures [68, 75]. The phase transition temperature of T_d and T_m was clearly specified from the dielectric loss curve. Table 17 summarizes the phase transition temperature of T_d and T_m, including the values of the dielectric constant of each peak, which were observed from the dielectric loss curve. Excluding the sample sintered at 950 °C, an increase of sintering temperature caused T_d to decrease and to dramatically decrease for samples sintered at high temperatures. In the case of T_m, it could not be observed from the sample sintered at 950 °C. An increase of sintering temperature caused T_m to experience a disorderly shift in the other samples. The dielectric constant at T_d (ε_d) and at T_m (ε_m) for various sintering temperatures are graphically presented in Figure 66. It can be seen that the value of ε_d is slightly higher than ε_m for sample sintered at 1,000 °C. The interval between ε_d and ε_m decreased when the sintering temperature increased to 1,050 °C. Thereafter, an increase of sintering temperature to 1,100 °C caused the value of ε_m to be slightly higher than ε_d. This interval increased when increasing the sintering temperature to 1,150 °C. The differences between ε_d and ε_m were calculated and are listed in Table 17. Park, et al. [83] suggested that the altitude of the dielectric constant peak at Curie temperatures and lower temperature are correlated with the grain core and grain shell, respectively, which is exhibited in the core-shell structure materials. The core-shell structure can be formed in ferroelectric ceramics such as BT and BNT which some cation additives [83]. The core-shell structure consists of relatively pure composition grain cores embedded in and surrounded by a second impurity phase grain shell [84]. In this study, the dielectric constant peak at T_m was indistinctly observed while the dielectric constant peak at T_d dominated for the sample sintered at a low temperature (Figure 65(a)). This suggests that the core-shell structure was formed in the system and the influence of the grain shell is higher than the grain core so the dielectric constant peak at T_d is more dominate than at T_m. By increasing sintering temperature, the dielectric constant peak at T_m seems more visible (Figure 65(b)-(c)). This suggests that the grain core was enlarger and grain shell was thinner. The sample sintered at 1,100 °C shows a dielectric constant peak at T_m more easily observed than the dielectric peak at T_d (Figure 65(d)). This indicated that the grain core is more highly influenced by the dielectric constant than the grain shell. This behavior was more distinctly exhibited in the sample sintered at 1,150 °C (Figure 65(e)). The enlarging of

the grain core and the thinning of the grain shell due to higher sintering temperature was probably due to with the higher evaporation of $Bi_{0.5}M_{0.5}TiO_3$ in Eq. 30.

The value of the dielectric constant and dielectric loss at room temperature (ε_r and tanδ) are listed in Table 16 and the variable of ε_r due to differences of sintering temperatures has been plotted as shown in Figure 66. By increasing sintering temperature from 950 to 1,000 °C, the ε_r tended to increase due to higher grain growth and densification. Thereafter, an increase of sintering temperature induced ε_r to decrease though the average grain size and density were enhanced. This can be attributed to the secondary phase affects. The value of ε_r was enhanced again when the sintering temperature was increased up to 1,150 °C. This was caused by the secondary phase being eliminated from the system. However, the low density due to the grains and grain boundaries being melted limited the ε_r value. Lu, et al. [12] reported the ε_r value of BNT with 10 mol% Li doped BNT, 16 mol% K doped BNT and BNKLT1610 ceramics prepared via the solid-state reaction method are 420, 480, 1,020 and 1,080, respectively. Nevertheless, these values are lower than the maximum ε_r of 1,210 obtained from this study. This demonstrates the potential for Li and K being substituted in BNT and the efficiency of the combustion technique for preparing BNKLT1610 ceramics.

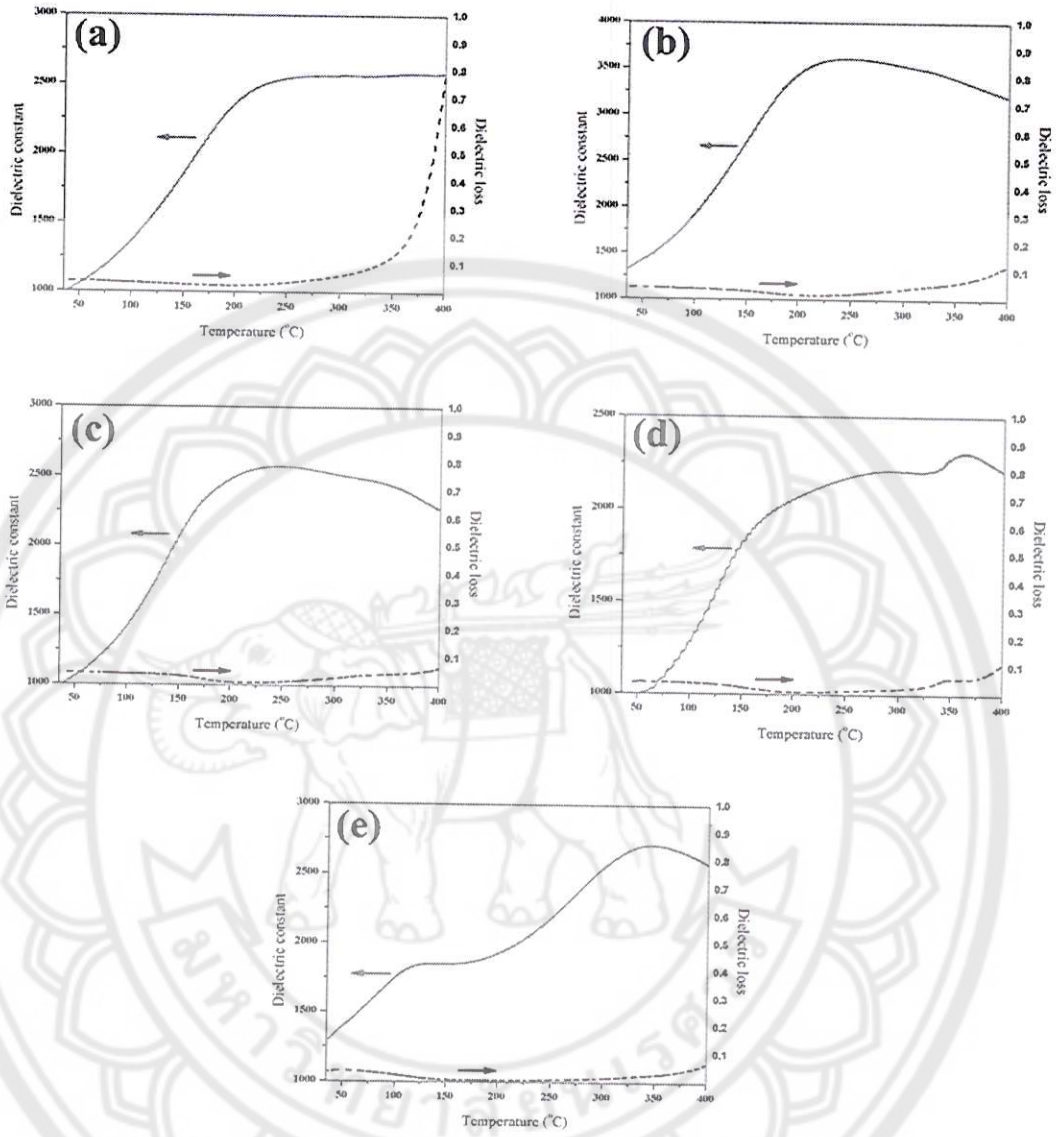

Figure 65 Temperature dependences of dielectric constant and dielectric loss of the BNKLT1610 ceramics sintered at; (a) 950 °C, (b) 1,000 °C, (c) 1,050 °C, (d) 1,100 °C and (e) 1,150 °C

Table 17 The T_d, T_m, ε_d, ε_m, $\Delta\varepsilon_{md}$, ε_r and tanδ of BNKLT1610 ceramics

Sintering temperature (°C)	T_d (°C)	T_m (°C)	ε_d	ε_m	$\Delta\varepsilon_{md}$	ε_r	tanδ
950	180	-	2,550	-	-	910	0.033
1,000	215	323	3,580	3,495	-85	1,210	0.036
1,050	204	330	2,530	2,490	-40	900	0.036
1,100	184	348	2,000	2,280	280	880	0.039
1,150	140	334	1,860	2,710	850	1,190	0.032

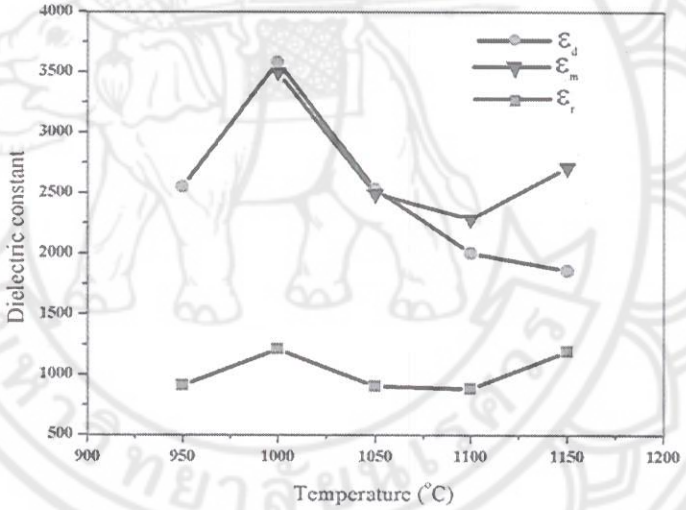

Figure 66 ε_d, ε_m and ε_r as function of sintering temperature of BNKLT1610 ceramics

Conclusions

Lead-free BNKLT1610 ceramics were successfully synthesized using the combustion technique. The effects of firing temperatures on phase formation, microstructure and dielectric properties were observed. The XRD revealed pure BNKLT1610 was produced when the calcination temperature was higher than 700 °C. Low calcining temperatures caused the volatilization of K_2O and a secondary phase

was formed. After being sintered between 950-1,150 °C, pure BNKLT1610 ceramics were obtained from the samples sintered at 950 °C and 1,150 °C. For the samples sintered at other temperatures, the secondary phase was repeatedly formed. An increase of sintering temperature from 950 °C to 1,100 °C enhanced grain size and densification while the sample sintered at 1,150 °C exhibited inferior morphology and a low density due to the evaporation of materials. The dielectric properties were highly influenced from the formation of the secondary phase and densification. Moreover, the grain core and grain shell formation highly influenced the variation of the dielectric constant values at phase transition points. The sample sintered at 1,000 °C shows the highest dielectric constant at room temperature (ε_r) and maximum dielectric constant (ε_m) with the values of 1,210 and 3,495, respectively. The sample sintered at 1,100 °C showed the highest densification but the formation of the secondary phase limited their dielectric properties. The highest value of ε_r in this study is significantly higher than those of other reports. This suggests the combustion technique effectively produces high quality BNKLT1610 ceramics.

CHAPTER VII

PHASE FORMATION, MICROSTRUCTURE AND DIELECTRIC PROPERTIES OF $Bi_{0.5}(Na_{0.74}K_{0.16}Li_{0.10})_{0.5}TiO_3$-$Ba(Zr_{0.5}Ti_{0.95})O_3$ CERAMICS PREPARED VIA THE COMBUSTION TECHNIQUE

Introduction

It is well known that BNT is a ferroelectric ceramic which possesses strong ferroelectricity [68]. However, the application for electronic devices of this material is limited by some problems such as its high coercive field, low piezoelectricity and low dielectric constant [19]. Therefore, other compositions or some cation additives were also added into BNT to improve their characteristics [72, 73]

Yang, et al. [70] modified BNT by substituting Na^+ by K^+ for 10-20 mol%. The result demonstrated that K-substitution induced the MPB region between rhombohedral–tetragonal phases at 18 mol% of K. This composition is very promising lead-free piezoelectric materials because it shows the optimum values of d_{33}, K_p, ε_r and tanδ of 144 pC/N, 0.29, 893 and 0.037, respectively. Lu, et al. [12] investigated the K^{1+} and Li^{1+} ion additive by replacing the Na^{1+} ion to form a BNKLT system. The study results suggested that the $Bi_{0.5}(Na_{0.74}K_{0.16}Li_{0.10})_{0.5}TiO_3$ or BNKL1610 composition showed the coexistence of a rhombohedral and tetragonal structure which is the MPB composition. The MPB composition led to a great enhancement in electrical properties compared with BNT. There was an increasing of d_{33} from 78 to 160 pC/N, an increasing of K_p from 0.16 to 0.35 and an increasing of ε_r from 420 to 1080. On the other view point, many researchers have reported BNT- improvement by introducing into the BNT-binary or ternary system chemical compositions such as BNT-BZT [17, 18], BNT-KNN [16] or BNT-BKT-BF [85, 86]. For example, Parija *et al.* [19] demonstrated doping BZT to BNT enhanced the ε_m from 1020 to 3533, d_{33} from 41 to 131 pC/N and P_r from 2.5 to 12 μC/cm^2 for 5 mol% BZT doped.

Recently, the idea of combining cation additives and the binary system of BNT-based solid solution to improve BNT properties has generated interest. Jarupoom, et al. [87] produced a system of (1-*x*)BNLT-*x*BT where 1.7 mol% La^{3+}

doped BNT and $0 \leq x \leq 0.10$. The ε_r and ε_{max} values of the BNLT–BT system were enhanced by the addition of BT fraction while T_c was lowered. Moreover, BT doping helped to reduce the tanδ of the ceramics at high temperature. The ε_r and ε_{max} showed maximum values of 1,615 and 4250 obtained from the BNLT with an addition of 10 mol% BZT.

In previous chapters, the research was focused on the investigation of $Bi_{0.5}(Na_{0.74}K_{0.16}Li_{0.10})_{0.5}TiO_3$ (BNKL1610) and $BaZr_{0.05}Ti_{0.95}O_3$ (BZT5) properties. The objective of this section is to investigat the possibilities of improving BNT properties by producing a new system of (1-x)BNKLT1610-xBZT5 or BNKLT-100xBZT ceramics. The effects of BZT fraction on phase formation, morphology and dielectric properties were also investigated. The samples were also synthesized through the combustion technique since this route has been shown t be an effective way to improve BNT and BZT properties [33, 88, 89].

Experimental procedure

The (1-x)BNKLT1610-xBZT5 ($x = 0.025 \leq x \leq 0.15$, step = 0.025) ceramics were synthesized using the combustion technique. Highly pure bismuth oxide (Bi_2O_3), sodium carbonate (Na_2CO_3), potassium carbonate (K_2CO_3), lithium carbonate (Li_2CO_3), titanium oxide (TiO_2), barium carbonate ($BaCO_3$) and zirconium dioxide (ZrO_2) were used as starting materials. Firstly, the raw materials were weighed according to the designed chemical formulae and were ball milled in an ethanol medium for 24 h. After being mixed with CH_4N_2O (fuel), the $Bi_{0.5}(Na_{0.74}K_{0.16}Li_{0.10})_{0.5}TiO_3$ (BNKLT1610) and $Ba(Zr_{0.05}Ti_{0.95})O_3$ (BZT5) were synthesized at 750 °C for 2 h and 1000 °C for 5 h, respectively. After calcination, the two synthesized powders were mixed with different values of x, milled once again, dried, and granulated by adding PVA. The granulated powders were pressed into disks of 15 mm diameter and then pressed using a uniaxial pressure of 80 MPa. These disks were sintered in air at 1100 °C for 2 h. The crystal structures of the ceramics were characterized by an X-ray diffractometer. The scanning electron microscopy (SEM) was employed to examine the microstructure of the sintered ceramics. The sintered disks were polished and had silver paste applied to both surfaces to measure their electrical properties. After applying the silver, the disks were fired at 600 °C for 5 min

and the temperature dependences of the dielectric properties were measured using a LCR meter.

Results and discussion

The X-ray diffraction patterns of the BNKLT-100xBZT ceramics with $0 \leq x \leq 0.15$ are shown in Figure 67. All of the BNKLT-BZT samples showed a pure perovskite phase which indicated that the BZT had completely diffused into the lattice to form a solid solution. Moreover, the diffraction peaks at 2θ of 44-48° at a very low scanning rate (step size 0.00116°, time/θ 7.42 s, and scan speed 0.05152°/s) showed interesting characteristics due to a significant change in the composition (Figure 67(b)). The investigation demonstrated that there are two features of diffraction patterns of interest. First, the diffraction peaks shifted to a lower angle when the BZT content increased. This suggested that the unit cells were stretched, which may be because the larger size Ba^{2+} (161 pm) occupies the A-site lattice by replacing Bi^{3+} (130 pm) and/or because the Na^{1+} (139 pm) and Zr^{4+} (72 pm) ion replaces the Ti^{4+} (61 pm) ion at the B-site lattice. The next diffraction feature of interest is the splitting of the (002) and (200) peaks. For BNKLT ceramics, the result of XRD patterns in the previous chapter demonstrated the coexistence of rhombohedral and tetragonal phases where the rhombohedral phase dominated. Additional BZT into BNKLT for BNKLT-2.5BZT induced an occurrence of a small hump at the left side of the (200) peak, indicating that the crystal structure was initially transformed to a tetragonal phase. The asymmetrical feature was distinctly observed when the BZT content was increased to 5 mol%. For BNKLT-7.5BZT composition, the diffraction peak appeared to split to (200) and (002) peaks. The splitting characteristic clearly observed when the BZT content was increased, which indicated that the tetragonallity tended to increase.

To understand the variation of unit cell volume due to a change in composition, the lattice parameters were also investigated. From the previous chapter, the BNKLT was assumed as a rhombohedral structure and the lattice parameter a was calculated. For BNKLT-BZT structure, the splitting of (002) and (200) peaks at 2θ of 44-48° was observed in BZT higher containing than 5 mol%. Therefore, the crystal structure of BNKLT-xBZT was assumed to be a rhombohedral and tetragonal structure for $x \leq 5$ mol% and $x > 5$ mol%, respectively. The lattice parameters, unit cell volume and c/a

ratio were calculated and are listed in Table 18. The calculation for the lattice parameters was based on different structures. The calculated lattice parameter *a* dramatically changed between BNKLT-5BZT (assumed as rhombohedral structure) and BNKLT-7.5BZT (assumed as tetragonal structure). However, it can be note that the lattice parameter *a*, lattice parameter *c*, unit cell volume and the *c*/*a* ratio also increased with an increasing BZT fraction. This observation supports the previous comment which stated that more BNT-doped leads to the enlargement of crystal unit cell volume.

The surface morphologies of BNKLT-*x*BZT ceramics were investigated and the results are shown in Figure 68. Normally, pure BNT exhibited cube-shape grain [ref]. Therefore, a characteristic of quasi-cubic morphology can be seen from the samples with a small amount of BZT in a BNKLT-BZT system (Figure 68(a)-(c)). In the case of BZT being higher than 7.5 mol%, the addition of BZT into the BNKLT matrix promoted the grain shape to slightly change from a cubic to a spherical grain (Figure 68(d)-(f)). The variation of average grain size due to its changing composition is listed in Table 18. The addition of BZT fraction on a BNKLT system affected the value of average grain size in the range of 1.43 – 1.89 μm.

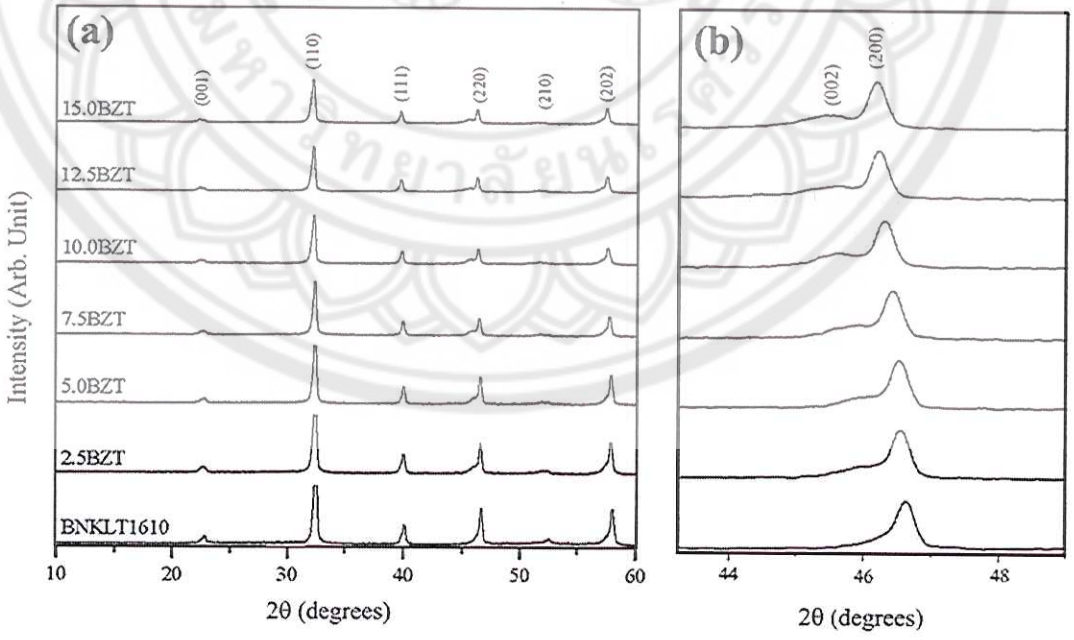

Figure 67 XRD patterns of BNKLT-100*x*BZT ceramics with $0 \leq x \leq 0.15$

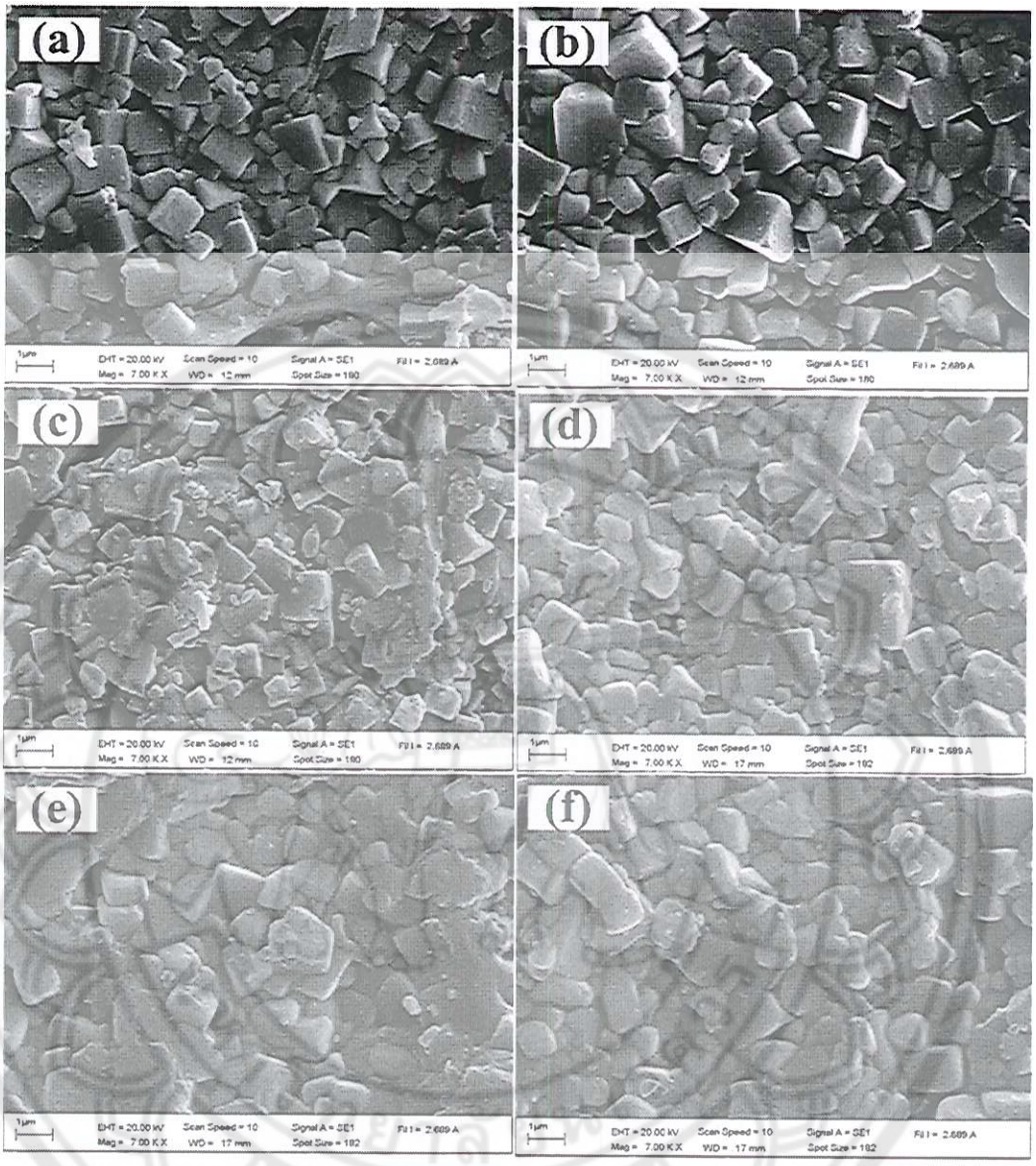

Figure 68 SEM photographs of surface of BNKLT-100*x*BZT ceramics; (a) $x = 0.025$, (b) $x = 0.050$, (c) $x = 0.075$, (d) $x = 0.100$, (e) $x = 0.125$ and (f) $x = 0.150$

Table 18 The lattice parameters *a* and *c*, unit cell volume, *c/a* ratio and average grain size of BNKLT-100*x*BZT ceramics

Samples	Lattice parameters		Unit cell Volume	*c/a* ratio	Average grain size
	a (Å)	*c* (Å)	(Å^3)		(μm)
BNKLT	3.432	-	-	-	1.72
BNKLT-2.5BZT	3.438	-	-	-	1.64
BNKLT-5.0BZT	3.449	-	-	-	1.89
BNKLT-7.5BZT	3.916	3.971	61.740	1.014	1.70
BNKLT-10.0BZT	3.926	3.986	62.368	1.015	1.43
BNKLT-12.5BZT	3.928	3.988	62.453	1.015	1.59
BNKLT-15.0BZT	3.927	3.991	62.560	1.016	1.44

The measured density with a variation in BZT content of BNKLT-100*x*BZTBZT is listed in Table 19. The density of the ceramics was in the range of 5.73–5.87 g/cm^3. The highest density was exhibited in BNKLT-12.5BZT. It can be observed that high density ceramics were obtained from the samples with high BZT content. In the previous chapter, the results indicated Bi and/or K and/or Na ions evaporate during the sintering process. This caused resulted in less dense samples. By the addition of BZT, evaporated ions can be substituted by more stable ions such as Na, and the volatility is reduced [89]. Therefore, the relative density is enhanced.

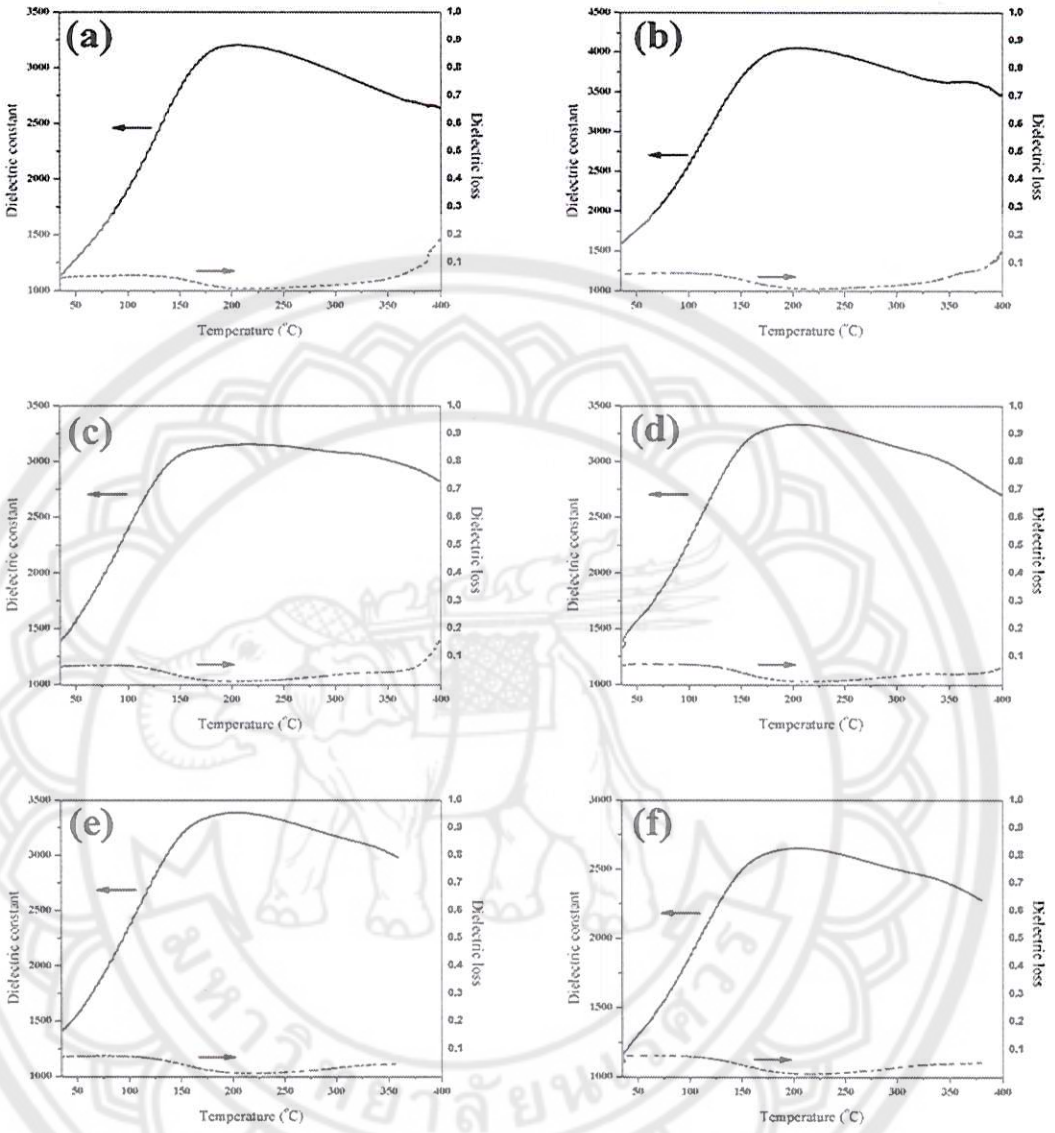

Figure 69 Temperature dependence of dielectric constant and dielectric loss of the BNKLT-xBZT ceramics with $0.025 \leq x \leq 0.15$

The dielectric constant and loss as a function of temperature for BNKLT-100xBZT ceramics is illustrated in Figure 69. For the sample with 2.5 mol% BZT (Figure 69(a)), the distinct dielectric peak with maximum value of dielectric constant occurs at ~200 °C. This point is referred to the dielectric peak in which the phase transition from a ferroelectric to an anti-ferroelectric phase at temperature called T_d. The dielectric curve shows an initial occurrence of another dielectric peak at a higher temperature (~360 °C). This point is clearly observed from the dielectric loss curve

and this point is referred to the dielectric peak in which the phase transition from anti-ferroelectric to paraelectric phase at temperature is called T_m. By increasing of BZT content to 5 mol%, the dielectric loss peak at T_m is more observed and shifted to a lower temperature (Figure 69(b)). The shifting of the dielectric loss peak at T_m tended move toward a lower temperature as the BZT content increased (Figure 69(c)-(f)). Increasing the BZT content only slightly affected the dielectric loss peak at T_d. However, the dielectric constant and dielectric loss could not be measured at high temperatures for BNKLT with 12.5 and 15 mol% BZT due to the dielectric constant and dielectric loss which was found to decrease and increase dramatically, respectively. This indicated that the materials exhibit high conductivity at high temperature, because the structure changed to paraelecric above Curie temperature [87]. The T_d, T_m, maximum dielectric constant (ε_{max}), dielectric constant at room temperature (ε_r) and dielectric loss at room temperature (tanδ) were observed and are listed in Table 19.

It can be noted that, an increase of BZT content caused the T_m to shift to a lower temperature. This is because the BZT has a lower value of paraelectric-phase transition temperature (~100 °C) [90] compared with that of BNKLT (~335 °C) [12]). In term of dielectric constant, the maximum dielectric constant was exhibited at the dielectric peak near T_d for all samples. This phenomenon shows the contrary behavior of the dielectric curve of BNT as reported in the literature [68, 75] in which the dielectric peak shows its higher altitude at T_m and its lower altitude at T_d. This can be attributed to the core-shell structure which was formed in the materials and because the shell grain was more highly influenced than the core grain as described in the previous chapter. The variation of ε_r and ε_{max} for various BZT contents are graphically presented in Figure 70. An increase of the BZT content led to both ε_r and ε_{max} to be enhanced and reach maximum values at 5 mol% BZT. Thereafter, ε_{max} suddenly dropped and then increased with an increase of BZT content until it reached 12.5% when it then decreased. Chu, et al. [43] reported that the MPB composition of BNT-BT is 6 mol% BT. Therefore, the highest values of ε_r and ε_{max} exhibited in the sample of BNKLT-5BZT may be attributed to this composition being near the MPB region of the BNKLT-BZT system. At the MPB region, the polarization vector can easily switch between all the allowed polarization orientations. Therefore, the dielectric properties

increased [91]. After dropping, ε_{max} tended to increase with increasing BZT content from 7.5 to 12.5 mol%. This result corresponds with the literature [92], which suggests that the dielectric constant of BNT-BT increase when the composition is near the tetragonal side of MPB region. However, the cause of reduction of ε_r and ε_{max} in BNKLT-15BZT sample is ambiguous.

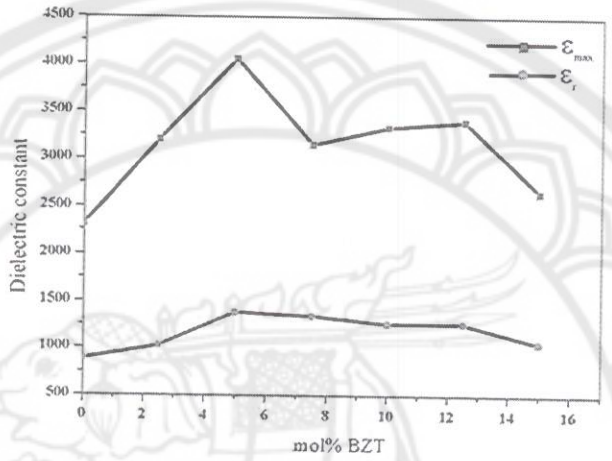

Figure 70 ε_r and ε_{max} as function of BZT fraction for BNKLT-xBZT ceramics with $0 \leq x \leq 0.15$

Table 19 Density, T_d, T_m, ε_r, ε_{max} and tanδ of BNKLT-100xBZT ceramics

Samples	density (g/cm^3)	T_d (^oC)	T_m (^oC)	ε_r	ε_{max}	tanδ at T_r
BNKLT	5.73	195	-	880	2,310	0.039
BNKLT-2.5BZT	5.81	190	-	1,020	3,200	0.045
BNKLT-5.0BZT	5.83	193	360	1,380	4,050	0.051
BNKLT-7.5BZT	5.79	191	330	1,340	3,150	0.061
BNKLT-10.0BZT	5.82	189	325	1,260	3,330	0.065
BNKLT-12.5BZT	5.87	190	320	1,260	3,390	0.068
BNKLT-15.0BZT	5.84	188	310	1,050	2,650	0.070

Conclusions

The effects of BZT content on phase formation, morphology and dielectric properties of BNKLT-100*x*BZT were studied. The XRD results demonstrated that the co-existence of the rhombohedral-tetragonal phase is exhibited for all samples. The addition of BZT content allowed the tetragonal phase to increase while the rhombohedral phase decreased. Moreover, the increase of BZT content caused the lattice parameters, unit cell volume and *c/a* ratio to increase. The SEM results suggested that the average grain size was slightly affected by the addition of BZT. However, the relative density tended to increase with increasing BZT fraction. After dielectric properties characterization had been employed, it was found that the addition of BZT caused T_m to shift to a lower temperature while T_d is insignificantly shifted. The appearance of the dielectric constant peak at T_d rather than at T_m was apparent for all compositions. This indicated that the grain shell has a higher influence than grain core in a BNKLT-BZT system. The maximum ε_r and ε_{max} with the values of 1,380 and 4,050 were observed from the sample with the composition BNKLT-5BZT. This can be attributed to the fact that this composition is located near the MPB region.